Global and Regional Sea Surface Temperature Trends

KENNETH S. CASEY

Oceanography Department, United States Naval Academy, Annapolis, Maryland

PETER CORNILLON

Graduate School of Oceanography, University of Rhode Island, Narragansett, Rhode Island

(Manuscript received 22 August 2000, in final form 5 February 2001)

ABSTRACT

Individual sea surface temperature (SST) anomalies are calculated using a satellite-based climatology and observations from the *World Ocean Atlas 1994* (WOA94) and the Comprehensive Ocean–Atmosphere Data Set (COADS) to characterize global and regional changes in ocean surface temperature since 1942. For each of these datasets, anomaly trends are computed using a new method that groups individual anomalies into climatological temperature classes. These temperature class anomaly trends are compared with trends estimated using a technique representative of previous studies based on 5° latitude–longitude bins.

Global linear trends in the data-rich period between 1960 and 1990 calculated from the WOA94 data are found to be 0.14° ± 0.04°C decade^{-1} for the temperature class approach and 0.13° ± 0.04°C decade^{-1} for the 5° bin approach. The corresponding results for the COADS data are 0.10° ± 0.03°C and 0.09° ± 0.03°C decade^{-1}. These trends are not statistically different at the 95% confidence level. Additionally, they agree closely with both SST and land–air temperature trends estimated from results reported by the Intergovernmental Panel on Climate Change. The similarity between the COADS trends and the trends calculated from the WOA94 dataset provides confirmation of previous SST trend studies, which are based almost exclusively on volunteer observing ship datasets like COADS.

Regional linear trends reveal a nonuniformity in the SST rates between 1945–70 and 1970–95. Intensified warming during the later period is observed in the eastern equatorial Pacific, the North Atlantic subtropical convergence, and in the vicinity of the Kuroshio extension. Also, despite close agreement globally, localized differences between COADS and WOA94 trends are observed.

1. Introduction

Of the many environmental parameters identified as priorities for climate change research by the Intergovernmental Panel on Climate Change (IPCC; Houghton et al. 1996), sea surface temperature (SST) is one of the more important. Understanding global SST changes is critical to climate change detection and attribution studies, initialization and validation of climate models, and the development of various emission scenarios and policies by which potential anthropogenic effects on global climate may be mitigated. Unfortunately, monitoring long-term changes in global SST is hindered by the size of the world ocean, changes in instrumentation, and the difficulty in taking measurements at sea.

Despite these difficulties, several studies have attempted to quantify changes in global SST over the last century. In 1981, Paltridge and Woodruff (1981) used Historical SST Data Project summaries of bucket and engine intake observations to estimate global SST trends and found a warming of approximately 0.6°C in the Northern Hemisphere and 0.9°C in the Southern Hemisphere between the 25-yr means of 1900–25 and 1945–70. However, this analysis did not account for the shift from uninsulated buckets to insulated buckets and engine intakes as the primary source of SST measurements. Folland et al. (1984) applied corrections to account for the changing measurement methods to the SSTs and nighttime marine air temperatures (NMAT) collected in the Met Office (UKMO) Main Marine Data Bank between 1856 and 1981 and found fluctuations of approximately 0.6°C. Satellite-derived multi channel SST estimates between 1982 and 1988 indicated a significant warming of 0.1°C yr^{-1} (Strong 1989), but the satellite retrievals used were shown to have been biased cold between April of 1982 and the end of 1983 by stratospheric aerosols released in volcanic eruptions of El Chichón (Reynolds et al. 1989).

In 1990, the IPCC released its first scientific assessment of climate change research (Houghton et al. 1990) and concluded that a warming of about 0.3°C had oc-

Corresponding author address: Kenneth S. Casey, Oceanography Department, United States Naval Academy, 572M Holloway Rd., Annapolis, MD 21401.
E-mail: casey@usna.edu

curred over the last century in the Northern Hemisphere oceans, and about 0.3°–0.5°C in the Southern Hemisphere (Folland et al. 1990). This conclusion was based on volunteer observing ship (VOS), buoy, and weather ship data collected since the late 1800s in an updated version of the UKMO dataset (Bottomley et al. 1990). Observations prior to 1942 were also corrected to account for the biases associated with the uninsulated buckets commonly used before World War II. The IPCC results agreed closely with the results of Farmer et al. (1989), which used the first release of the Comprehensive Ocean–Atmosphere Data Set (COADS; Woodruff et al. 1987). The COADS collection contained most, but not all of the UKMO observations. Improvements to COADS have resulted in a larger database with more unique observations than the UKMO database, but the majority of observations are duplicated in both collections (Woodruff 1990). An update to the IPCC report was published in 1992 (Houghton et al. 1992) and confirmed the earlier estimates of long-term SST warming at 0.45° ± 0.15°C in the last 100 yr (Folland et al. 1992). Parker et al. (1994) extended the analyses presented in the 1990 and 1992 IPCC reports and reached the same conclusions after incorporating more in situ data and adding satellite-based SSTs after 1982 into their climatology. Addressing the problem of limited data availability, Smith et al. (1994) employed optimal averaging techniques on the COADS data to estimate seasonal SST changes and found similar trends to previous studies, particularly in the relatively data-rich period since 1950. Their technique, however, had an advantage over simpler averaging techniques since it provided confidence intervals associated with the anomaly time series. In the IPCC's second major assessment (Houghton et al. 1996), revised bucket corrections (Folland and Parker 1995) and an improved climatology based on the 1961–90 reference period were used. The resulting SST trends closely resembled previous estimates. Recently, Strong et al. (2000) used satellite SST data alone to examine trends over a 13-yr period from 1984–96. They found significant regional trends and a global warming trend, but the time period of available data was too short to establish statistical significance on the global results.

The consistency of these SST trends is not surprising, considering the similar methods and datasets employed. Virtually all the previous studies have relied on ship-of-opportunity data collected into large databases like COADS (Woodruff et al. 1987, 1993, 1998) and the UKMO Historical SST data bank (Bottomley et al. 1990; Folland and Parker 1995). Furthermore, SST anomalies are commonly computed on 2° or 5° monthly grids, and similar procedures are used to calculate hemispheric and global anomaly trends from the monthly anomaly fields.

While these techniques have become the standard means of computing global SST trends, several issues make it worthwhile to consider alternative approaches. First, SST anomalies calculated on large grid cells are susceptible to noise introduced by SST variations across the binned region and time (Trenberth et al. 1992). Second, determining monthly anomalies using binned averages rather than using individual observations makes error estimation difficult since the standard error of the anomaly for an individual bin can not be directly calculated. Third, the in situ climatologies used are limited in their ability to represent some parts of the world ocean, particularly in the Southern Hemisphere where observations are scarce. Progress has been made by blending these climatologies with operational satellite SST (Reynolds and Smith 1995), but the operational nature of the satellite data reduces their potential accuracy and usefulness and the blending techniques result in varying base periods for different parts of the world ocean. Finally, all of the SST values used in previous studies have come from essentially the same dataset based on VOS observations.

Recent developments have provided an opportunity for calculating SST trends using a different technique that addresses these issues. A new global SST climatology based on Pathfinder Advanced Very High Resolution Radiometer (AVHRR) data and resolved to 9.28 km has been developed and shown to limit noise in individual SST anomalies better than in situ and blended SST climatologies (Casey and Cornillon 1999). An updated version of this ''Pathfinder+Erosion'' climatology is used to generate daily SST anomalies from individual SST observations. Calculating individual anomalies reduces the level of error introduced by SST variations within a bin and makes it possible to choose from a variety of binning strategies to determine global and regional SST trends. Additionally, the generation of individual anomalies rather than monthly binned values makes the direct calculation of anomaly standard errors possible regardless of the binning scheme. The Pathfinder dataset used to generate this climatology also provides more accurate SST estimates and uses all available satellite retrievals unlike the operational AVHRR data used in previous blended climatologies.

The release of the *World Ocean Atlas 1994* (WOA94) collection (Levitus and Boyer 1994) of high-quality research ship data provides an opportunity to address the concern that previous SST trends have been determined using similar collections of VOS data. The WOA94 dataset consists of SST observations from conductivity–temperature–depth (CTD) probes, hydrographic sampling bottles, expendable bathythermographs (XBT), and mechanical bathythermographs (MBT). Although substantially fewer in number than the COADS collection, the WOA94 observations provide a partially independent SST dataset with which previous estimates of SST trends can be compared. Since the second IPCC assessment, the COADS dataset has also been updated to include observations through 1995, and more observations have been digitized and included for earlier years as well.

These resources permit global and regional charac-

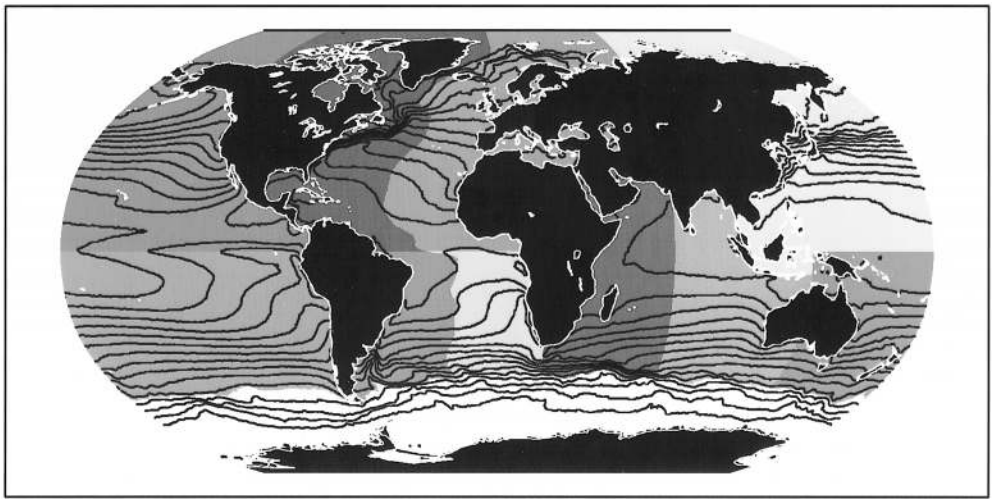

FIG. 1. Temperature classes and regions for binning anomalies. The contours outline every other temperature class as defined by the 13-yr mean Pathfinder+Erosion SST field.

terization of SST trends using independent datasets and different techniques. The datasets and analytical methods are described in section 2, and the results are presented in section 3. In section 4, the results of this study are discussed in the context of previous climate change research, and the novel aspects of this approach are examined.

2. Data and methods

a. Calculation of anomalies

The calculation of SST anomalies was performed using a technique similar to that used in Casey and Cornillon (1999). The advantage of Casey and Cornillon's approach compared with approaches that utilize regional averages (over 5° by 5° boxes, for example), is that it does not include the within-box variance of climatological SST in the resulting anomaly values. Two SST anomaly datasets were created, one from the WOA94 dataset and the other from the COADS collection. The WOA94 dataset contains high-quality surface temperature observations from CTD, XBT, MBT, and hydrographic sampling bottles. The COADS collection (Release 1b) consists primarily of engine intake and bucket measurements. The COADS dataset contains most of the WOA94 observations for the periods 1950–79 and after 1990, but the two datasets are independent during the other years. This study focuses on data collected after 1942, since older COADS observations require bias corrections to account for the systematic use of uninsulated buckets prior to World War II. Furthermore, a large percentage of the WOA94 observations were collected after 1942, making comparisons with COADS difficult in the earlier, data-sparse part of the century.

Point anomalies are determined by subtracting the Pathfinder+Erosion daily climatological SST from each of the WOA94 and COADS observations. The daily climatological SST is determined by simple linear interpolation between the nearest pentad climatological values. These pentad values are computed from 13 years of version 4 and 4.1 Pathfinder AVHRR SST data that are declouded using the standard cloud-masking procedures plus an additional erosion filter that further masks as cloudy any pixel immediately adjacent to a cloudy pixel. This satellite climatology is resolved to 9.28 km in space and 5 days in time, and is based on 1985–97 data. Missing pixels in the climatology are filled using the median SST of the surrounding 7×7 pixels. Both cubic spline and linear temporal interpolation routines were tested to fill the remaining gaps and found to have virtually identical results, so the simpler linear interpolation between pentad values approach is chosen. Each of the final pentad climatological SST fields is smoothed with a 7×7 median filter to reduce small-scale noise. This Pathfinder+Erosion climatology is an updated version of the one described in Casey and Cornillon (1999). Like the older climatology, this new Pathfinder+Erosion pentad SST climatology produces lower anomaly standard deviations than other SST climatologies.

In Casey and Cornillon (1999), the WOA94 anomalies were also subjected to a clustering procedure that averages observations nearly collocated in time and space to prevent them from being inappropriately weighted in subsequent areal averages. Significant computer processing time was required to perform the cluster analysis, so MBT observations were excluded from that study. In this analysis, tests showed that the clustering had no significant effect on global and regional trends computed without the MBT observations so the clustering procedure was not used. Addition of the MBT data also significantly improves the spatial and temporal coverage of the WOA94 dataset and nearly doubles the number of available anomalies. The COADS anomalies,

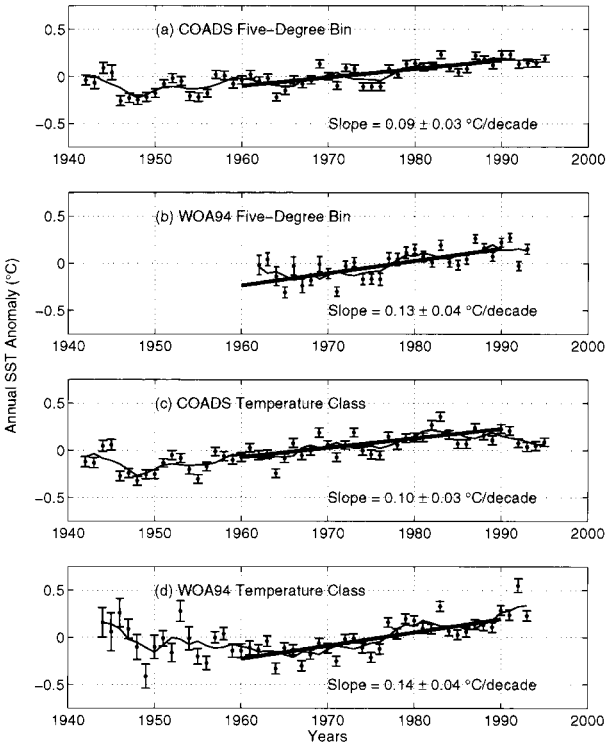

FIG. 2. Demeaned global annual SST anomaly trends with standard error bars for (a) COADS 5° bins, (b) WOA94 5° bins, (c) COADS temperature classes, and (d) WOA94 temperature classes. The thick line is a linear fit to the anomalies between 1960 and 1990, and its slope and standard deviation are indicated in the panel. The thin line indicates a 5-yr running mean.

owing to the large size of the dataset, were not clustered in Casey and Cornillon (1999), so the similar set of anomalies is used here.

Approximately 4.0×10^6 WOA94 and 88.5×10^6 COADS anomalies are created using these procedures. Anomalies with a magnitude greater than 8°C are excluded since they fall outside of physical limits, even in the eastern tropical Pacific where El Niño events cause large changes in SST (Parker et al. 1994). This step proved useful in eliminating obviously erroneous in situ SST observations.

b. Binning of anomalies

The above steps yield an SST anomaly associated with each in situ observation for both the WOA94 and COADS collections. These individual anomalies are then binned both to reduce the variance of the estimates and to allow for the calculation of trends at specific locations. Two different binning strategies are used. First, a slightly modified version of the binning scheme of Parker et al. (1994) is used. This approach, based on 5° bins, has been a common means of computing SST anomalies for the purpose of detecting SST trends. While more recent studies have improved upon this technique (Parker et al. 1995; Shen et al. 1998), use of this method permits a nearly direct comparison of these results with previous studies. As noted in the previous section, the method used to calculate anomalies in this study does not include the within-box variance, so the region over which the binning is performed should not matter *if* the warming or cooling trend is uniform over the region. As is evident from the results of this study, however, this is not the case; the rate of warming does vary over a basin. This means that if the region over which the anomalies are binned includes water warming at different rates the resulting estimate of warming will not reflect either rate accurately. The second approach to binning used in this study addresses this question. Specifically, we hypothesize that the rate of warming is water mass dependent and that water masses can be defined by their surface temperature. An extreme example of this idea is the Gulf Stream, which advects water from the south and then moves this water eastward into the basin. If the water to the south is warming more rapidly than that to the north, one would expect that the region encompassing the Gulf Stream would warm more rapidly than that on either side. In some cases atmospheric forcing may create anomalies that are not aligned with water masses, which suggests that an ideal analysis would be tailored to a set of naturally occurring anomaly patterns. A form of reduced space optimal interpolation (RSOI; Kaplan et al. 1997, 1998) in which the reduced space relates to the exclusion of noise from the covariance matrix eigenmodes used to construct the analysis could potentially be used. However, a global RSOI of individual SST anomalies using a covariance matrix calculated at the 9-km resolution of the Pathfinder dataset would be very computer intensive, and the satellite dataset may not yet span a sufficiently long period to calculate the covariance matrix. The water mass–based approach presented here divides the globe into 1°C temperature classes based on the 13-yr climatological SST and groups observations over large homogeneous regions of the ocean surface. This alternative binning scheme is investigated to determine its ability to reduce uncertainties and make better use of the available in situ data relative to the standard 5° bin method.

1) 5° SQUARES

In the approach representative of traditional techniques, monthly average SST values from the Met Office Historical SST dataset (MOHSST4; Bottomley et al. 1990) on a 5° grid are expressed as anomalies from a monthly 5° × 5° climatology (Parker et al. 1994). These anomalies are constructed using initial groupings of 1° in space and 5 days in time. In this study, the anomalies are calculated individually for each observation from the 9.28-km resolution Pathfinder+Erosion climatology and then averaged into monthly 5° bins. Following the steps described in section 2.1 of Parker

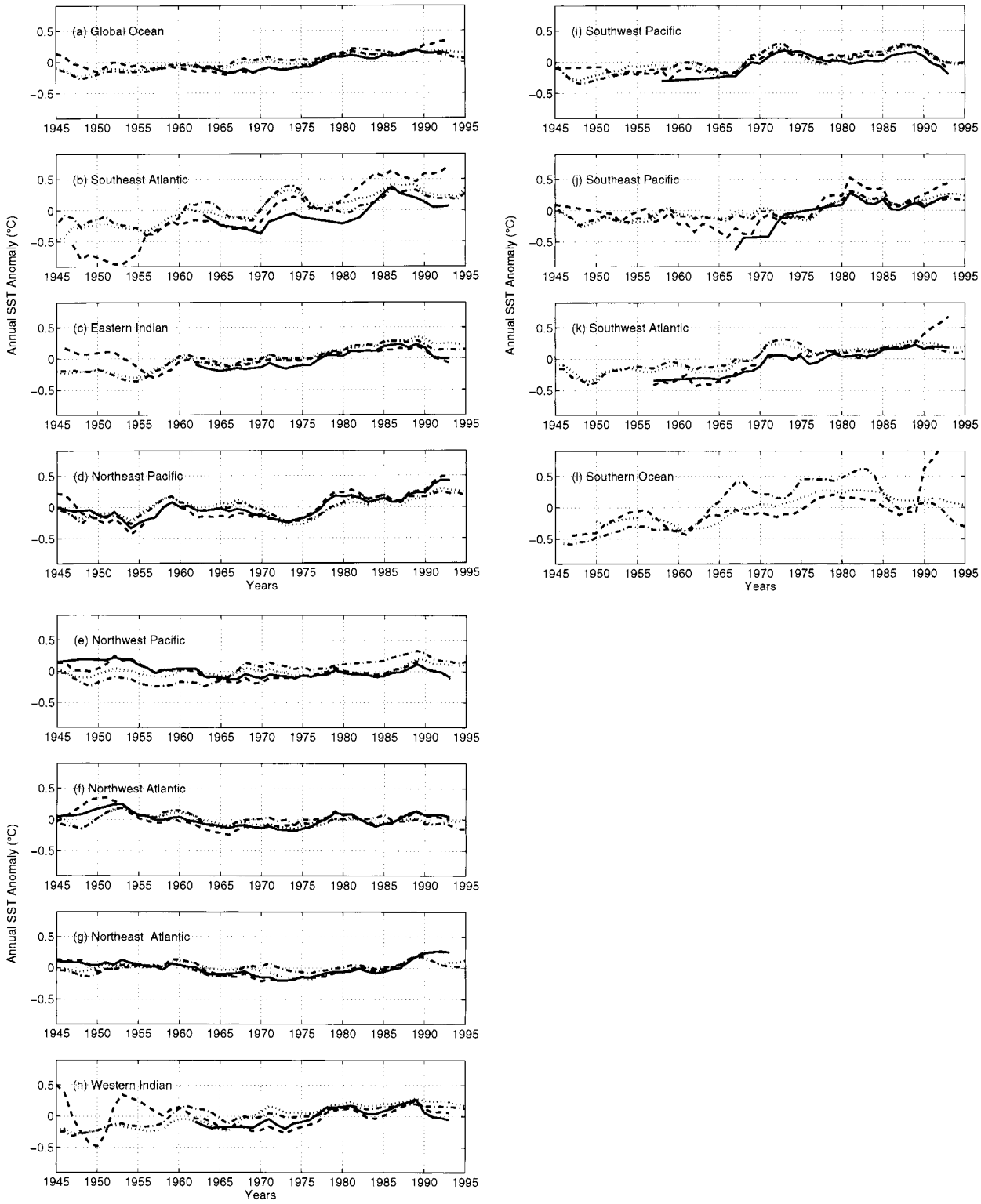

FIG. 3. Regional annual anomaly SST trends smoothed with a 5-yr running mean filter for COADS 5° bins (dotted), WOA94 5° bins (solid), COADS temperature classes (dash–dot), and WOA94 temperature classes (dashed) for the (a) globe, (b) southeastern Atlantic, (c) eastern Indian, (d) northeastern Pacific, (e) northwest Pacific, (f) northwest Atlantic, (g) northeast Atlantic, (h) western Indian, (i) southwest Pacific, (j) southeast Pacific, (k) southwest Atlantic, and (l) Southern Ocean regions.

TABLE 1. Global and regional linear SST trends (°C decade^{-1}) and std dev for 1960–90 for the COADS and WOA94 datasets and the 5° bin and temperature class binning schemes.

Region	COADS		WOA94	
	5° bin	T class	5° bin	T class
Global Ocean	0.09 ± 0.03	0.10 ± 0.03	0.13 ± 0.04	0.14 ± 0.04
Northwest Pacific	0.03 ± 0.03	0.15 ± 0.05	0.04 ± 0.04	0.07 ± 0.05
Northeast Pacific	0.03 ± 0.04	0.08 ± 0.04	0.12 ± 0.06	0.16 ± 0.07
Northwest Atlantic	0.00 ± 0.03	−0.01 ± 0.06	0.05 ± 0.04	0.08 ± 0.06
Northeast Atlantic	0.02 ± 0.03	0.06 ± 0.03	0.05 ± 0.04	0.05 ± 0.04
Western Indian	0.14 ± 0.05	0.05 ± 0.05	0.17 ± 0.08	0.15 ± 0.04
Eastern Indian	0.16 ± 0.04	0.15 ± 0.05	0.16 ± 0.06	0.12 ± 0.04
Southwest Pacific	0.12 ± 0.04	0.12 ± 0.05	0.07 ± 0.08	0.13 ± 0.06
Southeast Pacific	0.10 ± 0.04	0.11 ± 0.05	0.21 ± 0.14	0.21 ± 0.09
Southwest Atlantic	0.16 ± 0.05	0.12 ± 0.05	0.15 ± 0.07	0.19 ± 0.11
Southeast Atlantic	0.17 ± 0.06	0.09 ± 0.07	0.17 ± 0.14	0.32 ± 0.12
Southern Ocean	0.15 ± 0.06	0.12 ± 0.08	N/A	0.10 ± 0.06

et al. (1994), the average of the eight surrounding 5° bins is then calculated if at least four of them contained data and substituted into the central bin if the central anomaly is flagged as missing or different from the average by more than 2.25°C. Then, the average of the previous and next monthly anomalies is calculated if both are available and substituted if the central anomaly is missing or different from the average by more than 2.25°C. These two substitution steps are then repeated two more times, for a total of three iterations. Any bins initially missing an anomaly are reset to missing, and any remaining anomalies differing from the average of the neighboring bin anomalies by more than 2.25°C are set to missing, even if only one neighbor is available. Due to inadequacies in the climatologies used in Parker et al. (1994), some areas of the globe were then excluded from further analysis. Parker et al. (1994) removed 165°E–160°W south of 60°S, 120°–90°W south of 55°S, and 160°–120°W south of 50°S, where the resulting anomalies appeared unreliable. The Pathfinder+Erosion climatology does not suffer the same Southern Hemisphere limitations, thus no regions are removed in this study. Application of these steps to the individual COADS and WOA94 anomalies results in two sets of monthly, 5° bin mean anomalies.

2) TEMPERATURE CLASSES

Temperature classes are also used to group anomalies for areal averaging. A 13-yr global mean SST field is calculated from the Pathfinder+Erosion dataset and divided into 1°C temperature increments. Each SST anomaly is placed into one of these temperature classes based on the 13-yr climatological SST at the location of the observation. For example, if the climatological SST for a given observation is 18.5°C, then the anomaly was placed in the 18°–19°C temperature class. Temperature classes are defined over 11 regions of the globe (Fig. 1). Generally, each basin is divided into eastern and western portions, and northern and southern portions, except for the Indian Ocean, which is only separated into eastern and western divisions. The Atlantic Ocean is divided into eastern and western portions at the location of the Mid-Atlantic Ridge. A Southern Ocean region is defined between Antarctica and the 7°C isotherm. The individual WOA94 and COADS anomalies are collected separately into each temperature class and region on a monthly basis and averaged to yield a mean monthly temperature class anomaly.

c. SST trends

Regardless of the binning scheme, annual anomalies for the globe and each region are calculated by successive temporal and area-weighted averaging. First, seasonal anomalies are calculated by averaging together the January–March, etc., monthly anomalies within each temperature class or 5° bin. The seasonal anomalies are then averaged to yield an annual anomaly. One month is required for a seasonal mean and two seasonal values are required to compute an annual anomaly based on anomaly decay timescales of about three months (Frankignoul and Reynolds 1983).

Area-weighted averaging is then performed on the constituent temperature classes or 5° bins to yield an annual mean anomaly for each of the 11 regions of the globe. These regional anomalies are then area weighted and combined to determine a global mean for each year from 1942 to 1995 for COADS and 1942 to 1993 for the WOA94 observations. For both binning techniques, a regional annual anomaly is calculated only if 25% or more of the surface area of the region is represented. To calculate a global annual anomaly, regions covering at least 50% of the global surface area are required. Both sets of COADS trends and the WOA94 temperature class trends are insensitive to changes in these requirements, but the WOA94 5° bin anomalies are affected, especially in the relatively data-sparse years before roughly 1960. If these techniques are to be extended further back in time to the more data-sparse periods, then more rigorous restrictions should be developed. These steps provide a total of four global and regional

annual anomaly time series, one each for the COADS 5° bin, COADS temperature class, WOA94 5° bin, and WOA94 temperature class techniques.

Linear trends are fit to these anomaly time series for the data-rich period between 1960 and 1990. A chi-square fitting routine is used that returns the linear fit as well as uncertainty estimates on the slope and intercept, plus a goodness-of-fit parameter that can be used to judge the appropriateness of the linear model (Press et al. 1992). These uncertainty estimates take into account the standard errors of the annual anomalies (see below). Linear trends are also fit to the annual anomaly time series for each of the temperature classes in each of the regions to permit more detailed characterizations of the SST trends.

d. Error estimates

This study, by generating anomalies for individual observations, permits direct calculation of the random error since the variance for each of the monthly 5° bins or temperature classes is known. This approach is different from the one used for the decadal anomalies in Parker et al. (1994), which required an estimation procedure based on differences between a gridded anomaly and the anomalies in adjacent grid cells.

The variances in the approach presented here are combined first seasonally and then annually to yield random error estimates for the mean annual anomalies using a technique similar to that used by Smith et al. (1994) to calculate the variance of a large area composed of several smaller subareas each with a known variance. Here, the total variance for a seasonal anomaly is given by

$$\sigma_T^2 = \frac{1}{N^2}\left[\sum_{i=1}^{N} \sigma_i^2 + 2\sum_{i=1}^{N-1}\sum_{j=i+1}^{N} \mathrm{Cov}(x_i, x_j)\right], \qquad (1)$$

where σ_i^2 is the variance of each of the monthly anomalies used to compute the seasonal mean. Note that independence is assumed for each of the individual anomalies in the calculation of σ_i^2, though this is not strictly true. The appendix discusses this assumption in greater detail. Here $\mathrm{Cov}(x_i, x_j)$ is the covariance of the anomalies between months i and j. Between one and three months are used in each seasonal mean, thus N equals between one and three. The calculation is performed for each temperature class or bin and each season for all years between 1942 and 1995 for the COADS observations and between 1942 and 1993 for the WOA94 observations. The same procedure is then used to calculate the variance of the annual mean, using N equal to between 2 and 4 with σ_i^2 equal to the seasonal variances used in the mean. The variance associated with each regional mean annual anomaly is computed in the same manner, with N equal to the number of temperature classes or 5° bins available in the region. Similarly, the variance of each global annual mean anomaly is determined using the anomalies and variances of each of the available subregions. When computing the variance for the regional and global means, the σ_i^2 term in Eq. (1) is spatially weighted to account for the differing areal extents of the constituent temperature classes, 5° bins, or subregions.

3. Results

a. Global trends

The global annual anomaly trends for the two datasets and two binning techniques reveal warming trends for 1960–90 of between 0.09° ± 0.03°C and 0.14° ± 0.04°C decade^{-1} (Figs. 2a–d). The WOA94 trends are qualitatively larger than the COADS trends but the differences are not significant at the 95% confidence level. These trends and their associated uncertainties incorporate the variation between years as well as the uncertainty on the anomaly for a given year. Recalculating the uncertainties of the global trends after removing the within-year errors indicates that about 57% of the standard deviation on average can be attributed to interannual variations. The remaining 43% of the trend uncertainty is thus associated with the standard deviations of the individual annual anomalies. Recalculating the uncertainties of the regional trends in the same manner indicates that on average approximately 69% of their standard deviations can be attributed to interannual variations and 31% to the uncertainty of the individual annual anomalies. Improved techniques that reduce the uncertainty of the individual annual anomalies could thus result in large reduction of the error on the global trend estimates, though that reduction would be somewhat less than 31%–43% since some of the annual anomaly uncertainty is due to geophysical noise that cannot be eliminated with improved methods.

Annual anomalies determined using the two binning schemes on the COADS data have average standard errors of 0.04°–0.05°C. The 5° bin anomalies calculated using the WOA94 data have average standard errors of 0.06°C. The temperature class binning technique, however, allows the WOA94 anomalies to be calculated in the data-sparse period before 1962, where the 5° bin technique does not characterize a sufficient portion of the ocean surface and is thus unable to produce annual anomalies. These additional anomalies in the earlier part of the record increase the overall average standard error for the WOA94 temperature class anomalies to 0.07°C.

b. Regional trends

Regionally, while some discrepancies are apparent, the WOA94 and COADS anomalies generally have similar trends for 1960–90, regardless of the binning scheme used (Table 1). The large-scale patterns are also consistent with one another, with generally larger warming trends in the Indian and Southern Hemisphere basins, and the smallest levels of warming, and some cool-

TABLE 2. Global (G), Northern Hemisphere (NH), Southern Hemisphere (SH), and regional SST, NMAT, and air temperature over land (AIRT) studies. Collections like COADS and MOHSST are categorized as VOS SST.

Study	Result	Period	Region	Data
This study COADS 5° bin	0.09 ± 0.03°C 10 yr^{-1}	1960–90	G	VOS SST
This study COADS T class	0.10° ± 0.03°C 10 yr^{-1}	1960–90	G	VOS SST
This study WOA94 5° bin	0.13° ± 0.04°C 10 yr^{-1}	1960–90	G	Hydrographic
This study WOA94 T class	0.14° ± 0.04°C 10 yr^{-1}	1960–90	G	Hydrographic
Paltridge and Woodruff (1981)	0.06°C	1900–70[a]	NH	VOS SST
Paltridge and Woodruff (1981)	0.09°C	1900–70[a]	SH	VOS SST
Folland et al. (1984)	0.06°C	1856–1981	G	VOS SST
Folland et al. (1990)	0.30°C	1861–1989	NH	VOS SST[b]
Folland et al. (1990)	0.3°–0.5°C	1861–1989	SH	VOS SST[b]
Folland et al. (1992)	0.45° ± 0.15°C[c]	1861–1990	G	VOS SST[d]
Parker et al. (1994)	0.45° ± 0.15°C[c]	1861–1993	G	VOS SST[e]
Nicholls et al. (1996)	0.45° ± 0.15°C[c]	1861–1994	G	VOS SST[f]
Nicholls et al. (1996)	0.15°C 10 yr^{-1}[g]	1960–90	G	NMAT
Nicholls et al. (1996)	0.08°C 10 yr^{-1}[h]	1960–90	G	VOS SST
Molinari et al. (1997)	−0.21° ± 0.19°C 10 yr^{-1}	1969–93	38°–43°N, 66°–78°W	XBT SST
This study COADS T class	−0.15° ± 0.23°C 10 yr^{-1}	1969–93	8°–13°C T classes[i]	VOS SST
This study WOA94 T class	−0.07° ± 0.23°C 10 yr^{-1}	1969–93	8°–13°C T classes[i]	Hydrographic
Molinari et al. (1997)	0.14° ± 0.06°C 10 yr^{-1}	1969–93	17°–38°N, 66°–78°W	XBT SST
This study COADS T class	0.04° ± 0.20°C 10 yr^{-1}	1969–93	14°–27°C T classes[i]	VOS SST
This study WOA94 T class	0.12° ± 0.20°C 10 yr^{-1}	1969–93	14°–27°C T classes[i]	Hydrographic
Holbrook and Bindoff (1997)	0.04°C 10 yr^{-1}[j]	1955–88	39°–49°S, 141°–179°E	XBT and MBT
This study COADS T class	0.06° ± 0.09°C 10 yr^{-1}	1955–88	9°–17°C T classes[k]	VOS SST
This study WOA94 T class	0.10° ± 0.09°C 10 yr^{-1}	1955–88	9°–17°C T classes[k]	Hydrographic
Zheng et al. (1997)	0.024° ± 0.06°C 10 yr^{-1}	1951–90	30°–50°S, 160°E–175°W	VOS SST
This study COADS T class	0.09° ± 0.07°C 10 yr^{-1}	1951–90	8°–21°C T classes[k]	VOS SST
This study WOA94 T class	0.20° ± 0.08°C 10 yr^{-1}	1951–90	8°–21°C T classes[k]	Hydrographic
Luo et al. (1998)	0.16°C 10 yr^{-1}	1960–90	G	AIRT
Lau and Weng (1999)	0.023°C 10 yr^{-1}	1955–97	40°S–60°N	VOS SST

[a] The result is the difference between the 1900–25 25-yr mean and the 1945–70 25-yr mean.
[b] As described in Bottomley et al. (1990) and Farmer et al. (1989).
[c] Includes air temperatures over land.
[d] Combines the datasets of Bottomley et al. (1990) and Woodruff et al. (1987).
[e] Combines the datasets of Bottomley et al. (1990), Woodruff et al. (1987), and Parker et al. (1996).
[f] An updated dataset with improved bucket corrections from Folland and Parker (1995).
[g] Estimated for ocean regions from Fig. 3.1 in Nicholls et al. (1996).
[h] Estimated for ocean regions from Fig. 3.2 in Nicholls et al. (1996).
[i] Computed using these temperature classes in the northwest Atlantic region.
[j] Computed using data from the top 100 m.
[k] Computed using these temperature classes in the southwest Pacific region.

ing, in the North Atlantic and North Pacific basins. Note that the uncertainty of the WOA94 slopes is nearly always larger than the uncertainty of the COADS slopes, which were created using the more numerous ship-of-opportunity dataset. Using the 5° bin approach and the WOA94 anomalies, no trend in the Southern Ocean could be calculated because there were insufficient data available to cover 25% of the region. The temperature class approach with the WOA94 anomalies was, however, able to determine a trend.

All four anomaly time series tend to capture the same broad features of the warming trends. For example, the global trends show a very small trend between 1950 and 1970, with a stronger warming around 1975 (Fig. 3a). The southeastern Atlantic region shows a strong oscillation with a period of approximately 12 yr (Fig. 3b). The peaks around 1962, 1974, and 1986 are apparent in both the COADS and WOA94 data using both the 5° bin and temperature class approaches. The similarity in the shapes of these curves, given the independence of the two datasets, suggests that the patterns observed are real. The eastern Indian Ocean shows a smooth linear trend after 1965 (Fig. 3c) and the troughs and peaks in the northeastern Pacific trends appear in all four time series (Fig. 3d). The other regions (Figs. 3e–l) also show similar patterns, with the largest differences occurring before 1960 except for the Southern Ocean (Fig. 3l) where they occur after 1965.

The 5° binned data may also be averaged by longitude at a given latitude. Figure 4 shows the linear trends in SST determined for the period 1960–90 as a function of latitude for each of the 11 regions identified in Fig. 1. Although the rate of warming or cooling differs somewhat between the two datasets, the variation with latitude is quite similar. Furthermore, both COADS and WOA94 indicate warming at almost all latitudes (in some cases, one of the 5° latitudinal bands shows slight cooling) for the South Atlantic, the South Pacific, the Indian Ocean south of the equator, and the Southern Ocean. By contrast, each of the northern basins show

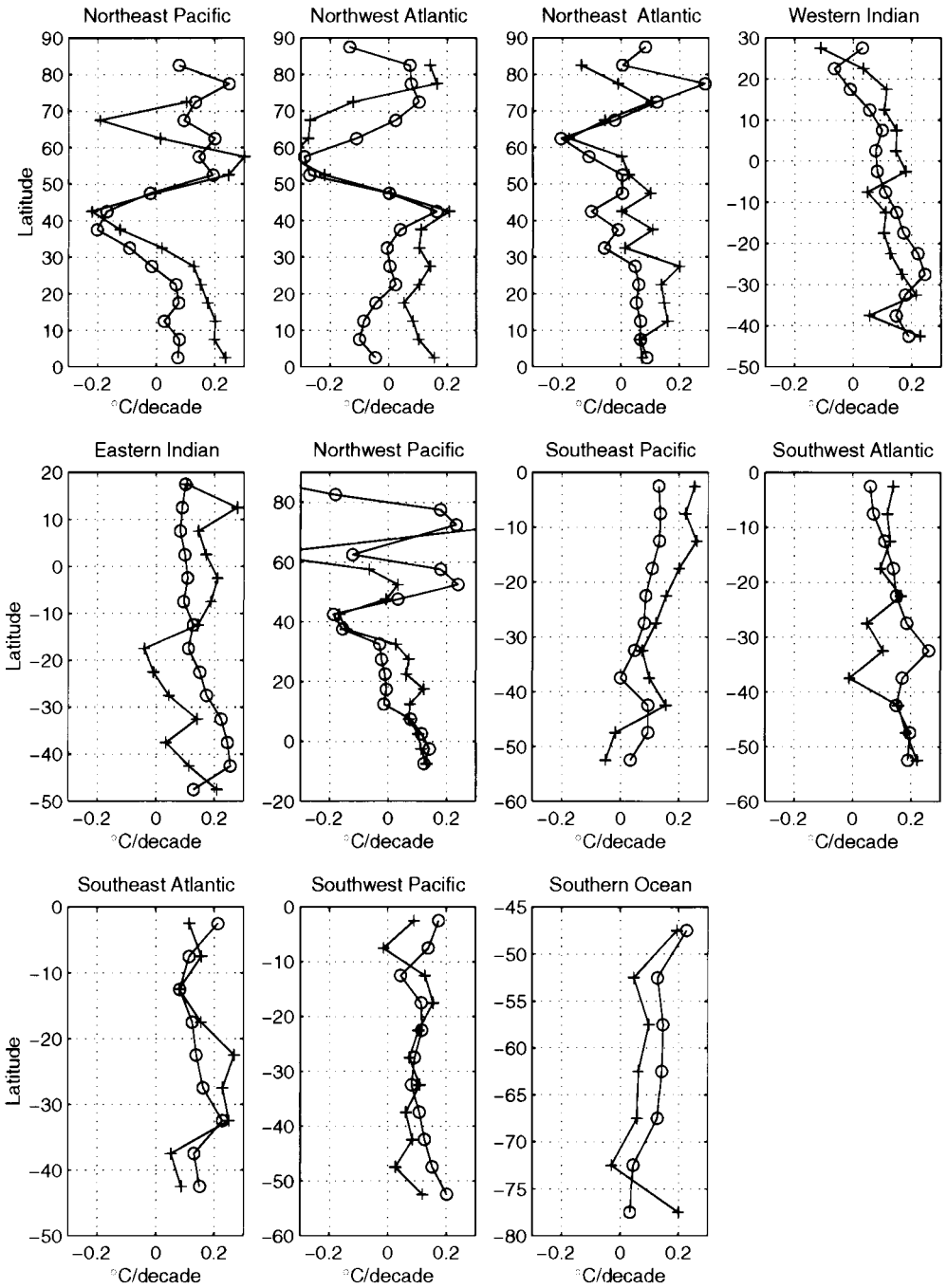

FIG. 4. COADS (o) and WOA94 (+) SST trends for 1960–90 obtained by averaging 5° bins by long for each of the regions indicated in Fig. 1.

significant cooling at mid and/or high latitudes, and this cooling is generally seen in the trends obtained from both datasets.

When viewed from the temperature class perspective (Fig. 5), the characteristics of the SST trends in the northwestern Atlantic and northwestern Pacific are very different from one another. For the COADS anomalies in the northwestern Atlantic, cooling trends are evident in temperature classes between 2°C (approximately 62°N when compared with latitudinal averages of Fig. 4)[1] and 7°C (approximately 45°N) and warmer than 21°C (approximately 35°N), while warming trends are seen

[1] At high latitudes the 2° and 7°C contours are oriented from southwest to northeast so the latitudes cited here are obtained by averaging across the region.

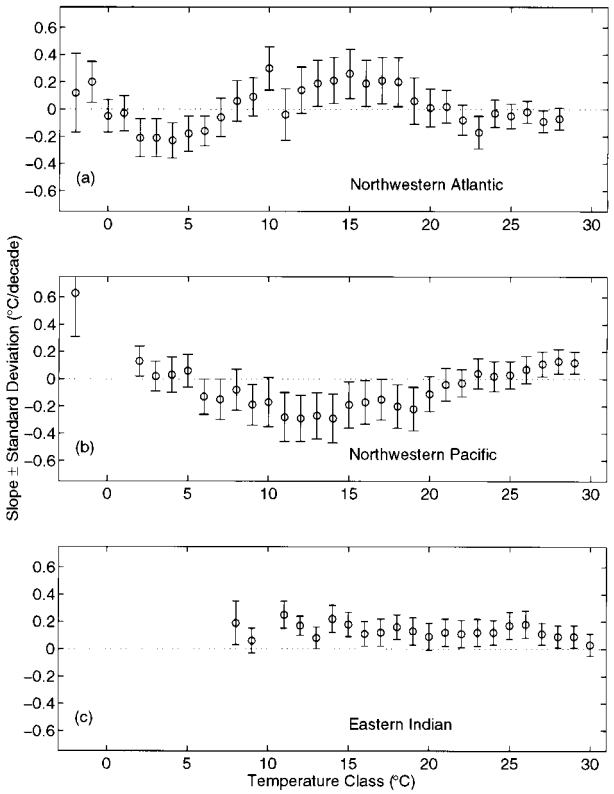

FIG. 5. The 1960–90 linear trends (°C decade^{-1}) of the COADS annual anomaly time series in each temperature class with error bars of std dev are shown for (a) the northwestern Atlantic, (b) the northwestern Pacific, and (c) the eastern Indian Oceans.

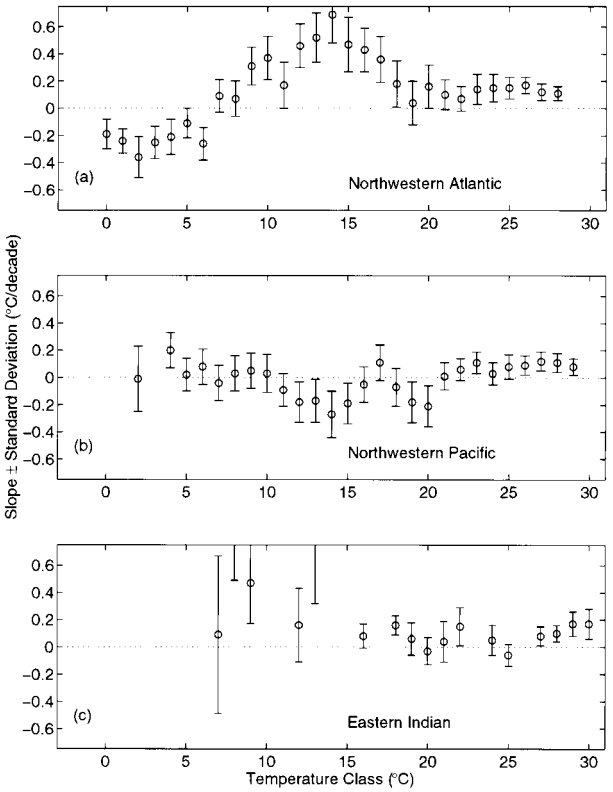

FIG. 6. The 1960–90 linear trends (°C decade^{-1}) of the WOA94 annual anomaly time series in each temperature class with error bars of std dev are shown for (a) the northwestern Atlantic, (b) the northwestern Pacific, and (c) the eastern Indian Oceans.

in the middle classes, 8°–21°C (Fig. 5a). The opposite pattern is reflected in the northwestern Pacific region, where cooling is seen in the middle temperature classes and warming trends are apparent in both the colder and warmer classes (Fig. 5b). As an aside, note that Fig. 5 compared with Fig. 4 clearly demonstrates the advantage of viewing these trends from different perspectives. The region of warming in the northwest Atlantic evident in the temperature class approach (Fig. 5) is largely missed in the approach using latitudinal bins (Fig. 4) because it occurs in a narrow region of relatively high SST gradient and because the region is not oriented zonally. The smooth transitions from warming to cooling and back are also difficult to see in the latitudinal averages. Finally, note that the small number of temperature classes that show warming at very high latitudes in the northwest Atlantic (Fig. 5) correspond to a relatively broad latitudinal range (Fig. 4). In all of the other regions, the SST trend is found to vary little with temperature class compared with these two regions. The eastern Indian Ocean is typical of the other regions (Fig. 5c).

The WOA94 anomalies have similar patterns in these regions. In the northwestern Atlantic (Fig. 6a), cooling trends in the cold classes are larger than those observed in the COADS data, as are the warming trends in the middle classes. The slight cooling in the warmest classes for the COADS anomalies is not seen in the WOA94 results, where the warm classes still have positive trends. The WOA94 northwestern Pacific trends (Fig. 6b) are similar to their COADS counterparts as well, but the differences in magnitudes are not as pronounced as they were in the Atlantic and the transition from warming in the colder classes to cooling in the middle classes is not as smooth. In the eastern Indian Ocean (Fig. 6c), relatively little variation is seen in the available temperature trends, similar to the pattern observed in the COADS data. Generally greater variability is seen in the WOA94 trends when compared to the COADS trends because of the fewer number of observations in the WOA94 dataset. This variability is evident in the colder classes of the eastern Indian basin, for example, where relatively few observations are available.

Figures 4, 5 and 6 show substantial variability in the SST warming and cooling trends when viewed both by temperature class and by latitudinal average. Figures 7 and 8 show global maps of the same data for the entire study period for COADS-derived trends (1942–95) and WOA94-derived trends (1942–93). Although these temperature trends are noisy, the patterns that emerge are

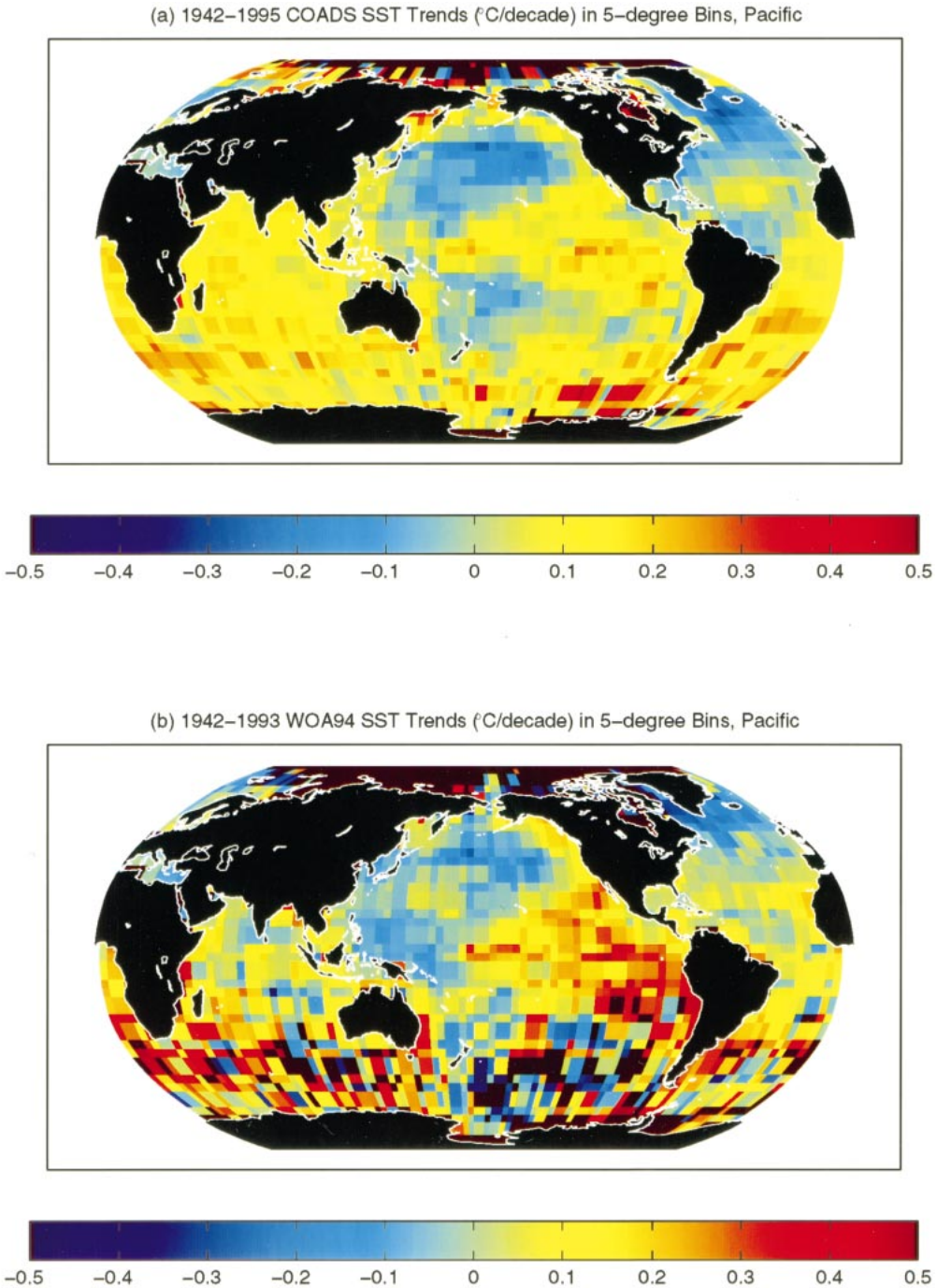

FIG. 7. Linear trends (°C decade^{-1}) by 5° bin in the Pacific Ocean for (a) COADS from 1942 to 1995 and (b) WOA94 from 1942 to 1993.

consistent between the two datasets for all ocean basins except for the Indian Ocean. For the Indian Ocean the COADS data show moderate warming and the WOA94 data show a mixture of slight warming and slight cooling. Both datasets show warming in the eastern equatorial Pacific and the South Atlantic and cooling in the subtropical convergence of the North and South Pacific basins and in much of the North Atlantic. These plots also suggest that, again with the exception of the Indian Ocean, warming trends obtained with the WOA94 data are generally higher than those obtained with the COADS data while cooling appears to be weaker in the

WOA94 data. The net result is the WOA94 data show a slightly higher rate of global warming when compared with the COADS data as noted earlier.

c. Nonuniformity of trends

Figures 7 and 8, based on the entire 54-yr record analyzed for this study, are consistent with previous work showing significant spatial variation in the rates of warming and cooling (e.g., Lau and Weng 1999; Parker et al. 1994). In other words, the surface of the ocean does not warm uniformly over the entire globe, but there are ''hotspots'' and ''coldspots'' where it warms and cools relatively faster. The trends for these figures were obtained, however, assuming a constant rate of warming or cooling for each 5° bin over the entire period. However, it is clear from Fig. 3 that the trends are not constant in time. Furthermore, the variability in these trends appears to differ from region to region. This suggests that global patterns of warming and cooling such as those presented in Figs. 7 and 8, will depend on the interval over which the trends were calculated. To gauge how significant the temporal change in nonuniformity is, 50 yr of the study interval were divided into two 25-yr periods: 1945–70 and 1970–95. Linear fits were made for each 5° bin for each of the two periods and examined for differences. Because of the paucity of data in the WOA94 dataset for the earlier years, only COADS data were considered for this part of the study.

The change in the nonuniformity of warming and cooling from one 25-yr interval to the next is visualized by differencing the demeaned fields of SST trends (Fig. 9). The demeaned fields were used because they define the nonuniformity of the warming and cooling for a given interval. Although somewhat noisy, especially in the Southern Hemisphere, clear patterns are evident. Specifically, the eastern equatorial Pacific, the subtropical convergence in the North Atlantic, and a region in the vicinity of the Kuroshio and Kuroshio extension in the western North Pacific show accelerating warming compared with most of the remainder of the ocean. Excluding those trends that do not pass the goodness-of-fit test in the chi-square fitting routine, the mean rate of warming over all 5° bins differed significantly between the two periods; for 1945–70 it is: $0.025° \pm 0.008$°C decade^{-1} while for 1970–95 it is: $0.086° \pm 0.006$°C decade^{-1}.

To test for the significance of the apparent clustering of relatively high or low trends in Fig. 9, a simple Monte Carlo experiment was undertaken. First, the mean and variance of the distribution of trends passing the goodness-of-fit test were calculated for each of the two temporal intervals. Then for each of 100 simulations, one number (one for each interval) was sampled from each distribution for each 5° bin on the globe and the resulting field obtained from the distribution corresponding to the first interval was subtracted from the field obtained for the second interval. For each simulation, the difference fields were demeaned following removal of bins that corresponded to an unacceptable fit or land in the observed data. The acceptable values for each simulation were then divided into one of three classes: 1) trend less than -0.075°C decade^{-1}, 2) trend greater than 0.075°C decade^{-1}, or 3) trend between -0.075°C and 0.075°C decade^{-1}. For each bin in class 1 or 2, the number of neighbors from the same class were counted. The result was for each simulation a set of numbers corresponding to the number of bins with 0 similar neighbors, 1 similar neighbor, . . . , to 8 similar neighbors. The same analysis was performed on the observed data (those trends from Fig. 9 that passed the goodness-of-fit test). The mean over the 100 simulations of the simulated results and the observed ''similar neighbor'' data are plotted in Fig. 10. It is clear from this plot that the clustering observed in Fig. 9 is not simply a statistical anomaly.

4. Discussion

Global and regional SST anomalies calculated using individual anomalies since 1942 have been presented. Both the COADS collection, which has been used in many previous studies of climatic SST changes, and the partially independent high-quality WOA94 observations reveal widespread warming trends over most of the world ocean for the years between 1960 and 1990. The discussion of these results begins with a comparison to the results of previous SST change studies in section 4a. The remaining sections focus on the new observations made in this study. Section 4b describes some of the advantages of the temperature class binning approach. Interesting differences between local trends obtained using the independent COADS and WOA94 datasets are explored in section 4c. Limitations of the current study and ideas for future improvements conclude the discussion and are presented in section 4d.

a. Comparisons with other trend estimates

Results from the previous global and regional climate change studies described in section 1 as well as several more recent studies are summarized in Table 2 to facilitate comparison to the results of this study. For the globe, the 1960–90 anomaly trends calculated using the COADS dataset are found to be $0.09° \pm 0.03$°C and $0.10° \pm 0.03$°C decade^{-1} for the 5° bin and temperature class averaging techniques, respectively. These trends closely match the approximately 0.08°C decade^{-1} trend for 1960–90 estimated from Fig. 3.2 in the IPCC's latest scientific assessment (Nicholls et al. 1996). The similarity is not surprising considering these values were all obtained using data that largely overlap with COADS observations. The close correspondence also indicates that the global trends calculated in the recent, relatively well-sampled years are insensitive to the spatial averaging method to within about 0.01°C decade^{-1}, and that

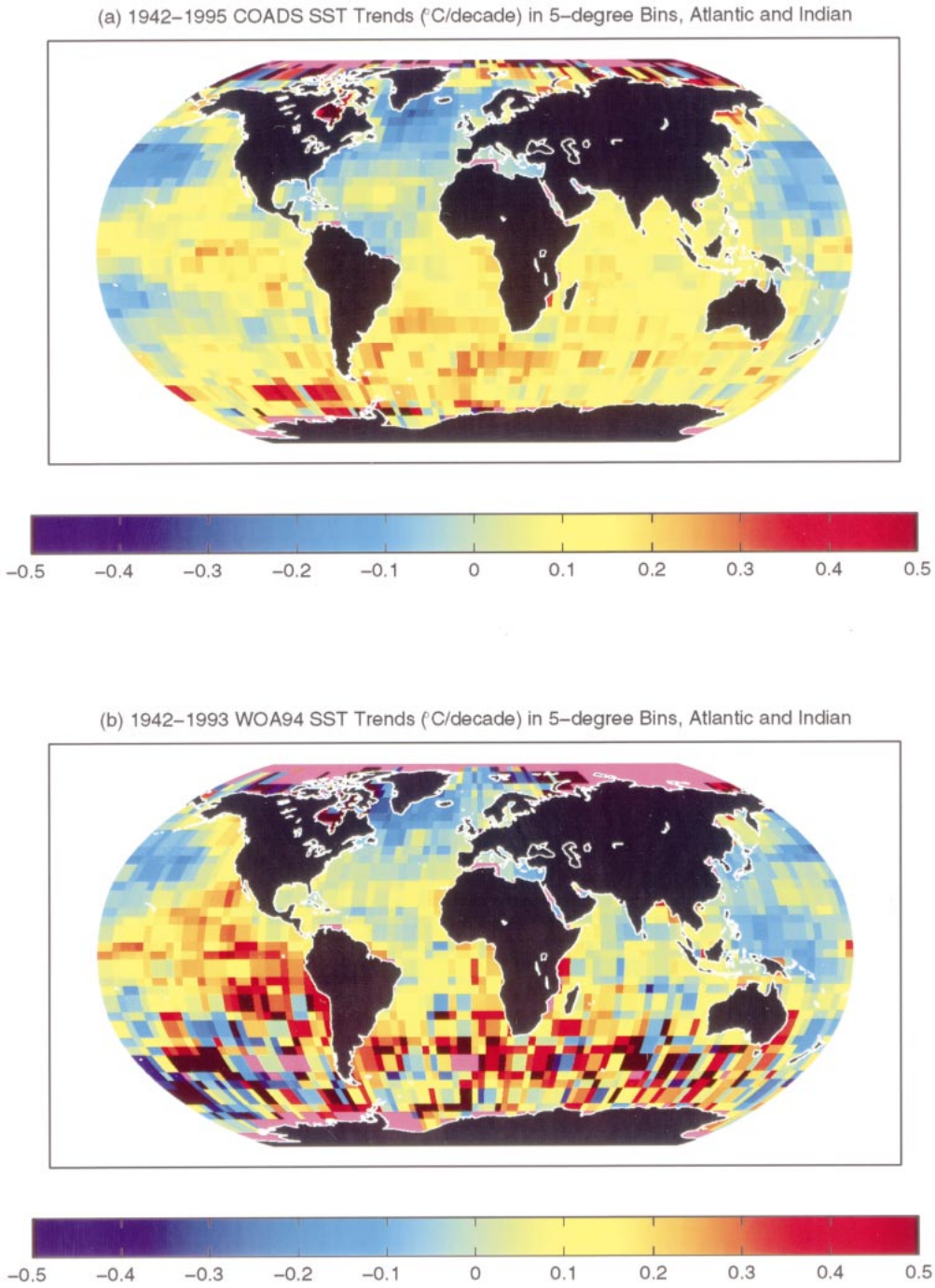

FIG. 8. Linear trends (°C decade^{-1}) by 5° bin in the Indian and Atlantic Oceans for (a) COADS from 1942 to 1995 and (b) WOA94 from 1942 to 1993.

the within-bin errors do not effect the magnitudes of the global trends, observations also made by Karl et al. (1994).

The partially independent WOA94 trends are also similar to the trends obtained from the COADS data. Qualitatively, the global WOA94 trends appear larger than the COADS trends but the differences are not significant at the 95% confidence level. The WOA94 trends, with magnitudes of 0.13° and 0.14°C decade^{-1}, provide an important dataset with which to compare the COADS results. The WOA94 trends are also similar to land–air temperature trends, which are estimated from

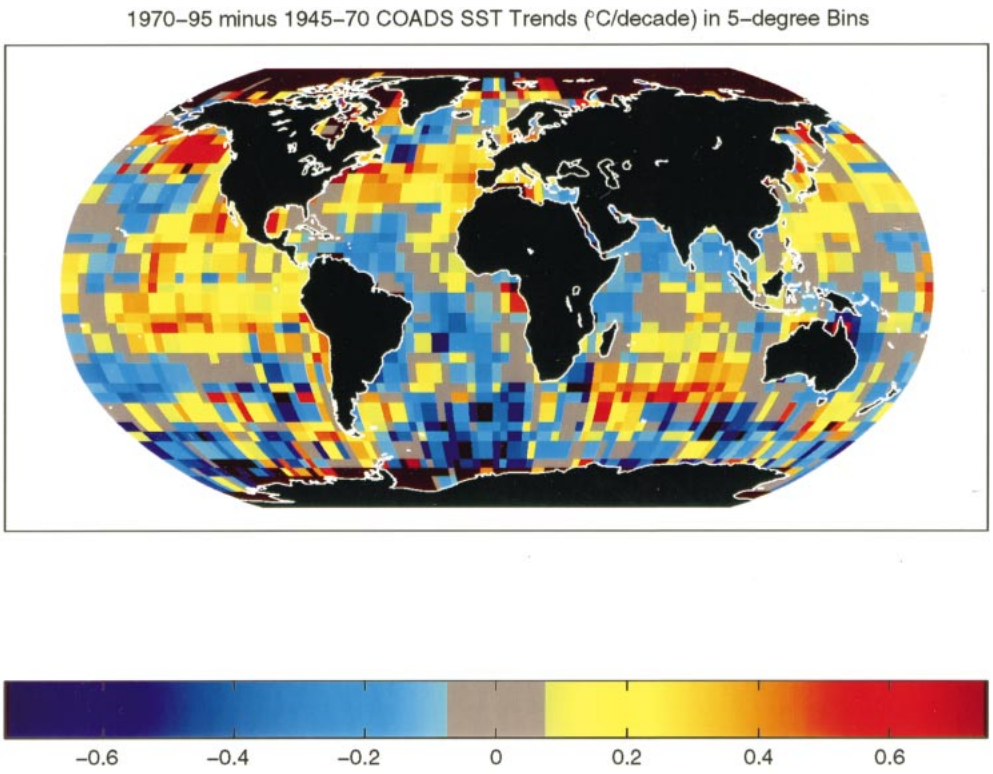

FIG. 9. The 1975–90 linear trends minus 1945–70 linear trends (°C decade^{-1}) by 5° bin for the Atlantic and Pacific Oceans.

Fig. 3.1 in Nicholls et al. (1996) to be approximately 0.15°C decade^{-1} between 1960 and 1990. For the same period, Luo et al. (1998) also found a warming trend of approximately 0.16°C decade^{-1} in December through February air temperatures over land using a smoothing spline analysis of variance technique to combine both spatial and temporal information in an optimal interpolation method. Note, however, that the year-round WOA94 trends and the winter season trends of Luo et al. (1998) may not be directly comparable since the air temperature trends over the Northern Hemisphere continents have been found to be greatest at this season (Nicholls et al. 1996). The similarity of these partially independent WOA94 and COADS results and their similarity to other measures of temperature change provide additional evidence in support of the observed warming trends.

The regional trends determined in this study also support observations made in previous studies. The midlatitude, middle temperature class cooling trends in the North Pacific observed here have been reported before, as has the cooling in the coldest temperature classes of the northern North Atlantic (Nicholls et al. 1996). The stronger warming trends in the Southern Hemisphere and Indian Ocean than the globe overall (Folland et al. 1990; Smith et al. 1994) are observed here as well. A strong oscillation with a period of about 12 yr in the southeastern Atlantic is seen clearly here, similar to the 15-yr oscillation seen by Venegas et al. (1996) and the 14–16-yr period in the strength of the subtropical anticyclone observed by Venegas et al. (1997). Mehta (1998) also identified a 12–13-yr oscillation in the Atlantic cross-equatorial SST gradient.

Comparisons with other recent studies that have investigated global and regional SST trends can also be made. Examining XBT data between 1969 and 1993 at several depths in the western North Atlantic, Molinari et al. (1997) found surface cooling trends of −0.21°C decade^{-1} north of the Gulf Stream from 38° to 43°N, with a standard deviation of 0.19°C. Between 17° and 38°N, they found a surface warming trend of 0.14° ± 0.06°C decade^{-1}. In an attempt to compare these results with the results of the present analysis, the northwestern Atlantic temperature class anomalies are examined. Temperature classes between 8° and 13°C are used to represent the region north of the Gulf Stream and classes between 14° and 27°C are used for the region south. Linear trends between 1969 and 1993 are determined from the average of the annual anomalies for each of the constituent temperature classes in each region. The COADS anomalies produced trends for the north region of −0.15° ± 0.23°C and 0.04° ± 0.20°C decade^{-1} for the south region. The trends determined from the WOA94 anomalies were −0.07° ± 0.23°C and 0.12° ± 0.20°C decade^{-1} for the north and south regions, respectively. Since these temperature classes extend to the

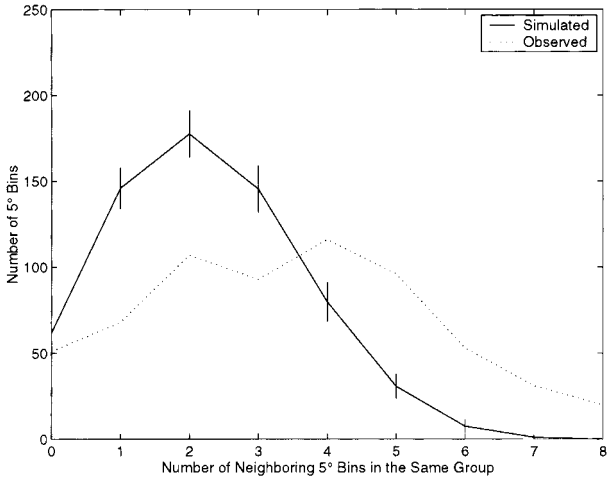

FIG. 10. Histogram of similar neighbors for two trend categories—greater than 0.075°C and less than −0.075°C decade^{-1}—in the 1970–95 minus 1945–70 trends. Solid line: Mean for 100 simulations with 1 std dev errors indicated. Dotted line: observed data.

Mid-Atlantic Ridge to the east they do not directly correspond to the trends presented by Molinari et al. (1997) that are narrowly confined between 66° and 78°W. However, both the WOA94 and COADS temperature class trends have the same sign as the XBT trends and the differences in magnitude are within the estimated uncertainties of the trends.

Using 10° by 10° resolution SST data provided by the National Oceanic and Atmospheric Administration/National Centers for Environmental Prediction and a complex Morlet wavelet transform, Lau and Weng (1999) determined a warming between 40°S and 60°N of approximately 0.10°C between 1955 and 1997. This warming translates into a trend over the 43-yr period of about 0.023°C decade^{-1}. In the present analysis, COADS anomalies between 1955 and 1995 yield global trends of 0.08° ± 0.02°C decade^{-1} using both the temperature class and 5° bin approaches. Global trends of 0.13° ± 0.03°C and 0.12° ± 0.03°C decade^{-1} are determined from the WOA94 anomalies up to 1993 using the temperature class and 5° bin techniques, respectively. These results indicate stronger warming trends than the Lau and Weng (1999) results and may occur because of the inclusion of all of the Southern Hemisphere data rather than restricting the domain between 40°S and 60°N.

In the vicinity of New Zealand from 39°–49°S to 141°–179°E, Holbrook and Bindoff (1997) found a warming trend in the upper 100 m of approximately 0.04°C decade^{-1} using XBT and MBT data between 1955 and 1988. The corresponding trends from this analysis were computed by averaging the 9°–17°C temperature class annual anomalies from the southwest Pacific region. For the COADS data, the trend is 0.06° ± 0.09°C decade^{-1} and the trend for the WOA94 anomalies is 0.10° ± 0.09°C decade^{-1}. These surface trends are comparable relative to the uncertainty level to the depth integrated results of Holbrook and Bindoff (1997). The greater magnitudes of the COADS and WOA94 trends may indicate stronger warming at the surface than in the top 100 m, but the differences are not statistically significant.

Also in the vicinity of New Zealand, Zheng et al. (1997) used an optimum statistical model that accounts for interannual variability associated with the Southern Oscillation to compute trends from the 5° by 5° UKMO ATLAS7 dataset. Between 30°–50°S and 160°E–175°W, the trend for 1951–90 was found to be 0.0239° ± 0.0551°C decade^{-1}. Corresponding trends from this analysis are determined using the average of the temperature class annual anomalies for the southwest Pacific classes between 8° and 21°C. The resulting COADS trend of 0.09° ± 0.07°C decade^{-1} is not significantly different, but the WOA94 trend of 0.20° ± 0.08°C decade^{-1} does differ substantially. The reason for this difference is not known, but may be related to the presence of large positive WOA94 trends off the east coast of Australia, evident in Fig. 7b.

b. Temperature class technique

The high quality of the Pathfinder+Erosion climatology coupled with the individual SST anomalies permits the use of a new binning strategy to group the data. These nontraditional bins are based on temperature classes defined by the 13-yr mean SST field calculated using the Pathfinder+Erosion climatology. These temperature class bins are found to produce 1960–90 trends that are similar to the trends computed using the 5° geographical bins representative of the techniques used in many previous studies. In the years before about 1970, when fewer observations are available, the temperature class approach produces similar anomalies but with smaller standard errors than the 5° binning scheme. Before 1962, the temperature class approach extends the more data-limited WOA94 anomalies farther back in time than was possible using the 5° bins. These results suggest that temperature classes could be used along with corrected pre-1942 COADS and WOA94 data to better characterize SST trends in the first half of this century. However, for this approach to be used to best advantage, corrections for individual COADS observations would have to be developed since current bias corrections are developed only for gridded SST observations (Folland and Parker 1995). Another advantage of the temperature class approach is its ability to reduce the monthly mean anomaly standard error relative to the 5° bin technique. This ability is illustrated in the appendix using a statistical efficiency parameter. Additionally, the temperature class approach provides a new perspective on warming trends as seen in the comparison between Figs. 5 and 4. The temperature classes reveal interesting features like the smooth transition between warming and cooling zones not evident in latitudinal averages.

c. Differences between COADS and WOA94 trends

Some interesting differences are apparent between the COADS and WOA94 temperature class trends within each of the regions of the globe (e.g., Figs. 5 and 6). While statistically significant warming trends are found mainly in the Southern Hemisphere for COADS, they appear throughout the global ocean for WOA94. The COADS trends tend to have smaller uncertainties because of the larger number of observations, but the trends also tend to be lower, which often makes them statistically indistinguishable from zero. Despite their larger uncertainties, the WOA94 trends are more often large enough to make them distinguishable from zero at the 90% confidence level (Figs. 7 and 8). Although the COADS and WOA94 global average trends are not statistically different because of the cumulative effect of averaging, locally over much of the globe there may be important differences. Several possibilities exist to account for these differences. There may be real geophysical differences between the quantities being measured by the COADS and WOA94 datasets. The COADS data generally come from ship intakes, which tend to be several meters below the surface. The WOA94 observations collected by research ships using MBTs, CTDs, XBTs, and hydrographic sampling bottles generally come from closer to the surface, near a depth of 1 m. While all of these measurements are within the surface layer, it is possible that the warming rates vary over the top several meters of the ocean. To test this idea, all of the WOA94 trends were recalculated using the individual observations measured at a depth of 10 m. The differences were small and not statistically significant. This result suggests that the top 10 m of the ocean are warming similarly, and that differences in the average depth of observation between the COADS and WOA94 collections are not a factor.

Another possible source of the differences between the COADS and WOA94 results could be undocumented biases, which may exist within either or both the COADS and WOA94 datasets between 1960 and 1990. For example, MBTs dominate the WOA94 dataset in the 1960s while XBTs dominate the 1980s. If the MBTs tend to yield slightly cooler SSTs than the XBTs, an artificial warming trend will be introduced. Similarly, biases of this type might exist within the COADS collection after 1942, when the now well-documented shift from bucket to engine intake temperatures occurred.

d. Limitations and ideas for future trend studies

This study is limited, as are all other studies of global SST changes, by the availability of in situ SST observations. The use of a satellite-based climatology and the development of a temperature class binning strategy optimizes the ability of the available data to represent sparsely sampled regions of the globe. Efforts must be made, however, to increase the in situ data coverage, particularly in the Southern Hemisphere and away from established shipping lanes if the uncertainty of SST trends in those regions is to be reduced.

Aside from increasing the in situ data coverage, improvements and extensions to the analysis presented here could be made. The regional trend estimates could be improved by accounting for significant climate patterns, as in the Zheng et al. (1997) analysis. The temperature class approach could also be developed further. For example, the longitudinal extent of the Pacific basins may warrant their division into more than two east–west regions as was done here. This approach may better resolve changes in SST trends across the Pacific. Some improvements could also be expected by including all of the WOA94 observations in the COADS datasets. While the WOA94 SST dataset is only about 5% of the size of COADS, it consists of generally higher-quality data. Combining the two, and augmenting them with additional recently digitized and collected observations would help reduce the uncertainties and improve the coverage. Improvements to the satellite climatology could also be made, particularly near ice edges and in the warm, tropical regions where the Pathfinder algorithm encounters difficulties from water vapor and aerosol contamination (Casey and Cornillon 1999). Extending the SST time series farther back in time would be beneficial, and would provide additional insight into the ability of the temperature class binning technique to provide smaller uncertainties in the more data-limited periods. To do this, however, corrections to the individual COADS measurements prior to 1942 are needed, and a careful investigation into possible changing biases in the WOA94 dataset would also have to be undertaken. Another area for development would be to apply the techniques developed here at several standard depth levels using the WOA94 temperature profile data and the WOA94 standard level climatologies to examine temperature changes at depth across the world ocean. Recently, Levitus et al. (2000) presented the results of a similar idea, using an update to the WOA94 dataset to examine changes in heat content for the world ocean. Between the mid-1950s and mid-1990s, they found a heat content change for the surface to 300 m that corresponds to a temperature change of 0.31°C. While fewer observations are available at depth, there are also lower noise levels than at the surface so studies like these could potentially extract useful trends for much of the globe.

Acknowledgments. This research was performed with support from NASA (NAGW3009) and salary support to P. Cornillon from the State of Rhode Island and Providence Plantations. Support to K. Casey was provided by the Universities Space Research Association and the Commander, Naval Meteorology and Oceanography Command. The Pathfinder data were obtained from the NASA Physical Oceanography Distributed Active Archive Center at the Jet Propulsion Laboratory, California

Institute of Technology. John Merrill of URI/GSO and Steve Worley of the National Center for Atmospheric Research Data Support Section provided the COADS data. Their assistance is greatly appreciated. We also thank the NODC Ocean Climate Laboratory for their efforts in compiling the WOA94 dataset. The authors also wish to thank David Parker and an anonymous reviewer for numerous suggestions that greatly improved this manuscript.

APPENDIX

Statistical Efficiency of Binning Schemes

The relative ability of the two averaging methods to minimize standard errors can be gauged by comparing the mean variances of anomalies and number of observations in monthly temperature class bins with those for 5° bins to give a measure of the ''statistical efficiency.'' This statistical efficiency is defined as σ_5^2/σ_t^2, the ratio of the 5° bin mean variance to the temperature class mean variance. The statistical efficiency indicates that for both the WOA94 and COADS datasets, the larger temperature class bins can be used to cover greater portions of the ocean surface yet still result in smaller standard errors on the monthly mean anomalies. For the WOA94 data, the ratio of the 5° bin mean variance to the temperature class mean variance is 0.49, indicating that within an average temperature class there must be more than 2.04 times as many observations as are found within an average 5° bin to achieve a smaller standard error, σ^2/N. The temperature class approach for the WOA94 data is found to have 2.47 times as many observations as are found for the 5° bin technique, indicating that the uncertainty associated with a temperature class is on average smaller than with a 5° bin even though a temperature class generally covers a significantly larger surface area than a 5° bin. For the COADS data, the variance ratio is 0.67, so an average temperature class would need only 1.49 times as many observations as an average 5° bin to reduce the standard error. Over 4.73 times as many observations are found in the temperature classes, strongly supporting the temperature class technique's ability to reduce the standard error of the monthly means.

The statistical efficiency parameter assumes that each of the observations are independent. While the sizes of the full WOA94 and COADS datasets preclude a calculation of the true number of independent samples in each grouping, an estimate can be made using a subset of the WOA94 data and the clustering procedure described in Casey and Cornillon (1999). The clustering routine averages closely packed observations in space and time and is performed after excluding MBT observations from the WOA94 dataset. Recomputing the statistical efficiency using this clustered dataset results in a variance ratio of 0.52, thereby requiring 1.92 times as many observations in a temperature class than in a 5° bin on average. For the clustered results, 2.22 times as many observations are found, again supporting the ability of the temperature classes to reduce the standard error. Individual temperature classes with few observations will likely have high standard errors due to their large spatial extents that incorporate greater spatial variations in the SST anomalies. These greater uncertainties are reflected in the computed trends, as in the cold temperature classes of the eastern Indian Basin shown in Fig. 6c. On average, however, the temperature class bins are better able to reduce the standard errors of the monthly mean anomalies than the 5° bins.

REFERENCES

Bottomley, M., C. Folland, J. Hsiung, R. Newell, and D. Parker, 1990: Global ocean surface temperature atlas (GOSTA). Joint Meteorological Office/Massachusetts Institute of Technology Project, Tech. Report, HMSO, London, England, 24 pp. and 313 plates.

Casey, K. S., and P. Cornillon, 1999: A comparison of satellite and in situ based sea surface temperature climatologies. *J. Climate,* **12,** 1848–1863.

Farmer, G., T. Wigley, P. Jones, and M. Slamon, 1989: Documenting and explaining recent global-mean temperature changes. Final report to NERC. Climate Research Unit Tech. Rep. Contract No. GR3/6565, Norwich, United Kingdom, 141 pp.

Folland, C., and D. Parker, 1995: Correction of instrumental biases in historical sea surface temperature data. *Quart. J. Roy. Meteor. Soc.,* **121,** 319–367.

——, ——, and F. Kates, 1984: Worldwide marine temperature fluctuations 1856–1981. *Nature,* **310,** 670–673.

——, T. Karl, and K. Vinnikov, 1990: Observed climate variations and change. *Climate Change: The IPCC Scientific Assessment,* J. Houghton, G. Jenkins, and J. Ephraums, Eds., Cambridge University Press, 195–238.

——, ——, N. Nicholls, B. Nyenzi, D. Parker, and K. Vinnikov, 1992: Observed climate variability and change. *Climate Change 1992: The Supplementary Report to the IPCC Scientific Assessment,* J. T. Houghton, B. A. Callander, and S. K. Varney, Eds., Cambridge University Press, 135–170.

Frankignoul, C., and R. Reynolds, 1983: Testing a dynamical model for mid-latitude sea surface temperature. *J. Phys. Oceanogr.,* **13,** 1131–1145.

Holbrook, N. J., and N. L. Bindoff, 1997: Interannual and decadal temperature variability in the southwest Pacific Ocean between 1955 and 1988. *J. Climate,* **10,** 1035–1049.

Houghton, J. T., G. J. Jenkins, and J. J. Ephraums, Eds., 1990: *Climate Change: The IPCC Scientific Assessment.* Cambridge University Press, 365 pp.

——, B. A. Callander, and S. K. Varney, Eds., 1992: *Climate Change 1992: The Supplementary Report to the IPCC Scientific Assessment.* Cambridge University Press, 205 pp.

——, L. G. Meira Filho, B. A. Callander, N. Harris, A. Kattenberg, and K. Maskell, Eds., 1996: *Climate Change 1995: The Science of Climate Change.* Cambridge University Press, 572 pp.

Kaplan, A., Y. Kushnir, M. Cane, and M. Blumenthal, 1997: Reduced space optimal analysis for historical data sets: 136 years of Atlantic sea surface temperatures. *J. Geophys. Res.,* **102,** 27 835–27 860.

——, M. Cane, Y. Kushnir, A. Clement, M. Blumenthal, and B. Rajagopalan, 1998: Analyses of global sea surface temperature 1856–1991. *J. Geophys. Res.,* **103,** 18 567–18 589.

Karl, T. R., R. W. Knight, and J. R. Christy, 1994: Global and hemispheric temperature trends: Uncertainties related to inadequate spatial sampling. *J. Climate,* **7,** 1144–1163.

Lau, K.-M., and H. Weng, 1999: Interannual, decadal-interdecadal,

and global warming signals in sea surface temperature during 1955–97. *J. Climate,* **12,** 1257–1267.
Levitus, S., and T. Boyer, 1994: *Temperature.* Vol. 4, *World Ocean Atlas 1994, NOAA Atlas NESDIS 4,* 117 pp.
——, J. I. Antonov, T. P. Boyer, and C. Stephans, 2000: Warming of the world ocean. *Science,* **287,** 2225–2229.
Luo, Z., G. Wahba, and D. R. Johnson, 1998: Spatial-temporal analysis of temperature using a smoothing spline ANOVA. *J. Climate,* **11,** 18–28.
Mehta, V. M., 1998: Variability of the tropical ocean surface temperatures at decadal–multidecadal timescales. Part I: The Atlantic Ocean. *J. Climate,* **11,** 2351–2375.
Molinari, R. L., D. A. Mayer, J. F. Fester, and H. F. Bezdek, 1997: Multiyear variability in the near-surface temperature structure of the midlatitude western North Atlantic Ocean. *J. Geophys. Res.,* **102,** 3267–3278.
Nicholls, N., G. V. Gruza, J. Jouzel, T. Karl, L. Ogallo, and D. Parker, 1996: Observed climate variability and change. *Climate Change 1995: The Science of Climate Change,* J. Houghton et al., Eds., Cambridge University Press, 133–192.
Paltridge, G., and S. Woodruff, 1981: Changes in global surface temperature from 1880 to 1977 derived from historical records of sea surface temperature. *Mon. Wea. Rev.,* **109,** 2427–2434.
Parker, D. E., P. Jones, C. Folland, and A. Bevan, 1994: Interdecadal changes of surface temperature since the late nineteenth century. *J. Geophys. Res.,* **99,** 14 373–14 399.
——, C. K. Folland, and M. Jackson, 1995: Marine surface temperature: Observed variations and data requirements. *Climatic Change,* **31,** 559–600.
——, ——, A. C. Bevan, M. N. Ward, M. Jackson, and K. Maskell, 1996: Marine surface data for analysis of climatic fluctuations on interannual-to-century time scales. *Natural Climate Variability On Decade-to-Century Time Scales,* D. G. Martinson et al., Eds., National Academy Press, 241–252.
Press, W. H., S. A. Teukolsky, W. T. Vetterling, and B. P. Flannery, 1992: Modeling of data. *Numerical Recipes in C.* 2d ed. Cambridge University Press, 656–706.
Reynolds, R. W., and T. M. Smith, 1995: A high-resolution global sea surface temperature climatology. *J. Climate,* **8,** 1571–1583.
——, C. K. Folland, and D. E. Parker, 1989: Biases in satellite-derived sea-surface-temperature data. *Nature,* **341,** 728–731.
Shen, S. S., T. M. Smith, C. F. Ropelewski, and R. E. Livezey, 1998: An optimal regional averaging method with error estimates and a test using tropical Pacific SST data. *J. Climate,* **11,** 2340–2350.
Smith, T. M., R. W. Reynolds, and C. F. Ropelewski, 1994: Optimal averaging of seasonal sea surface temperatures and associated confidence intervals (1860–1989). *J. Climate,* **7,** 949–964.
Strong, A., 1989: Greater global warming revealed by satellite-derived sea-surface-temperature trends. *Nature,* **338,** 642–645.
——, E. Kearns, and K. Gjovig, 2000: Sea surface temperature signals from satellites—An update. *Geophys. Res. Lett.,* **27,** 1667–1670.
Trenberth, K. E., J. R. Christy, and J. W. Hurrell, 1992: Monitoring global monthly mean surface temperatures. *J. Climate,* **5,** 1405–1423.
Venegas, S. A., L. A. Mysak, and D. N. Straub, 1996: Evidence for interannual and interdecadal climate variability in the South Atlantic. *Geophys. Res. Lett.,* **23,** 2673–2676.
——, ——, and ——, 1997: Atmosphere–ocean coupled variability in the South Atlantic. *J. Climate,* **10,** 2904–2920.
Woodruff, S., 1990: Preliminary comparison of COADS (US) and MDB (UK) ship reports. *Observed Climate Variations and Change: Contributions in Support of Section 7 of the 1990 IPCC Scientific Assessment,* D. Parker, Ed., WMO/UNEP, XXVII.1–XXVII.36.
——, R. Slutz, R. Jenne, and P. Steurer, 1987: A comprehensive ocean–atmosphere data set. *Bull. Amer. Meteor. Soc.,* **68,** 1239–1250.
——, S. Lubker, K. Wolter, S. Worley, and J. Elms, 1993: Comprehensive Ocean–Atmosphere Data Set (COADS) Release 1a: 1980–92. *Earth Syst. Monit.,* **4,** 1–8.
——, H. Diaz, J. Elms, and S. Worley, 1998: COADS Release 2 data and metadata enhancements for improvements of marine surface flux fields. *Phys. Chem. Earth,* **23,** 517–526.
Zheng, X., R. E. Basher, and C. S. Thompson, 1997: Trend detection in regional-mean temperature series: Maximum, minimum, mean, diurnal range, and SST. *J. Climate,* **10,** 317–326.